Kinetics of parametric instabilities of Alfvén waves: Evolution of ion distribution functions

Lorenzo Matteini, Simone Landi, Marco Velli, Petr Hellinger

Kinetics of parametric instabilities of Alfvén waves: Evolution of ion distribution functions

Lorenzo Matteini,[1] Simone Landi,[2] Marco Velli,[3] and Petr Hellinger[4]

Received 16 October 2009; revised 14 March 2010; accepted 26 March 2010; published 14 September 2010.

[1] Using numerical simulations in a hybrid regime, we studied the evolution of large-amplitude Alfvén waves subject to modulational and decay instabilities, including the effects of ion kinetics. We considered both a monochromatic and incoherent spectrum of waves, different wave polarizations and amplitudes, and different plasma regimes, ranging from $\beta < 1$ to $\beta > 1$. We found in all cases that ion dynamics affects the instability evolution and saturation; as a feedback, wave-particle interactions provide a nonlinear trapping of resonant particles that importantly change the properties of the ion velocity distribution functions. In particular, we observed a proton acceleration along the magnetic field and in some cases the formation of a parallel velocity beam traveling faster than the rest of the distribution. For the range of parameters used in our simulations, the fundamental ingredient in generating an ion beam is observed to be the parallel electric field carried by the density fluctuations driven by the ion-acoustic modes generated by the parametric instabilities.

Citation: Matteini, L., S. Landi, M. Velli, and P. Hellinger (2010), Kinetics of parametric instabilities of Alfvén waves: Evolution of ion distribution functions, *J. Geophys. Res.*, *115*, A09106, doi:10.1029/2009JA014987.

1. Introduction

[2] A class of wave-wave interactions characterizing the propagation of finite-amplitude Alfvén waves, are the so-called parametric instabilities [see, e.g., *Hollweg*, 1994, and references therein]. In these nonlinear processes, a mother wave (also called a pump wave) couples to a compressive acoustic-like perturbation (or ion-acoustic quasi-mode) and other electromagnetic fluctuations, leading to different parametric instabilities, depending on the plasma characteristics.

[3] Probably the best known parametric process is the decay instability [e.g., *Sagdeev and Galeev*, 1969; *Goldstein*, 1978; *Derby*, 1978], which involves the excitation of a compressive wave having a larger wave vector k_s than the mode k_0 of the pump wave. In this interaction the energy is gradually transferred from the mother wave to the acoustic unstable wave, which then grows in amplitude, and to another daughter (or reflected) Alfvén wave with $k_r < k_0$. This three-wave interaction satisfies the lower sideband condition $k_r = k_0 - k_s$, so the daughter wave is always backward propagating.

[4] The parametric decay is believed to play a role in many space plasmas where Alfvén waves are often observed [*Belcher and Davis*, 1971], because it provides a natural mechanism for production of backward propagating waves. In the solar wind plasma, an increase of the ratio between sunward and antisunward propagating Alfvén waves is observed with increasing distance [*Bavassano et al.*, 2000; *Bruno and Carbone*, 2005].

[5] Another process that can generate density fluctuations is the modulational instability [e.g., *Hasegawa*, 1970, 1972; *Lashmore-Davies*, 1976; *Mio et al.*, 1976; *Mjolhus*, 1976]; in this case, compressive modes are destabilized by the modulation of the pump-wave magnetic field intensity, which occurs at a wavelength larger than that of the pump wave ($k_s < k_0$), owing to the generation and interaction with two daughter Alfvén waves propagating in the same direction as the mother wave (lower and upper sidebands $k = k_0 \pm k_s$).

[6] Growth rates of parametric instabilities depend on the mother wave properties, amplitude and polarization, and the plasma condition, mainly the plasma beta. The Hall-MHD fluid approximation [e.g., *Longtin and Sonnerup*, 1986] predicts the left-handed polarized Alfvén wave to be decay and modulationally unstable for $\beta < 1$, while the right-handed Alfvén wave results are decay unstable for $\beta < 1$ and modulationally unstable when $\beta > 1$.

[7] A large literature exists about numerical studies on the propagation of Alfvén waves for different plasma conditions in the fluid MHD [e.g., *Umeki and Terasawa*, 1992; *Ghosh et al.*, 1993; *Malara and Velli*, 1996; *Malara et al.*, 2000; *Del Zanna et al.*, 2001; *Del Zanna*, 2001] and Hall-MHD frameworks [*Hoshino and Goldstein*, 1989]. However, the consequences of kinetic effects on parametric instabilities can be important, in particular, because they change the saturation dynamics of the processes and should be taken

[1]LESIA, Observatoire de Paris, Meudon, France.
[2]Dipartimento di Astronomia e Scienza dello Spazio, Università degli Studi di Firenze, Firenze, Italy.
[3]Jet Propulsion Laboratory, California Institute of Technology, Pasadena, California, USA.
[4]Astronomical Institute, Academy of Sciences of the Czech Republic, Prague, Czech Republic.

0148-0227/10/2009JA014987

Table 1. Initial Conditions for Different Simulations[a]

Run	β_p	β_e	Polarization	$\delta B/B_0$
A	0.01	0.1	L	0.05
B	0.01	0.1	R	0.05
C	0.01	0.1	L	0.1
D	0.01	0.1	L	0.3
E	0.01	0.1	L	0.5
F	0.01	0	L	0.05
G	0.1	4	R	0.5
H	0.08	0.5	L	0.2
I	0.1	1	L	0.1
J	1	1.5	L	0.2
K	1.5	2	L	0.5
L	1.5	2	R	0.5

[a]The mother wave is a monochromatic large-amplitude Alfvén wave with wave vector $k_0 = 0.2$. For each simulation, we report the proton and electron plasma beta, the wave polarization (L, left; R, right), and the amplitude.

into account. These were studied analytically by *Inhester* [1990] and through the use of numerical simulations by *Terasawa et al.* [1986] and *Vasquez* [1995] in past years and more recently by *Nariyuki et al.* [2007] and *Araneda et al.* [2007]. The results of these studies suggest that, in general, ion kinetics reduce the instability growth rates with respect to the fluid predictions and at the same time enlarge the range of the unstable mode, leading to additional decay- or modulation-type instabilities for modes that are stable in fluid theories.

[8] How the collisionless saturation of parametric instabilities also influences particles that contribute to the dynamics and their distribution function has been only marginally investigated. In a recent paper, *Araneda et al.* [2008] showed how the trapping driven by a parametric modulational instability, in a monochromatic case, can generate a velocity beam in the proton distribution. In this work, we extend their investigation and we discuss the dynamics in a large range of parameters. The result of *Araneda et al.* [2008] is then confirmed by the present analysis. Moreover, we find that not only modulational but also decay instabilities can produce proton velocity beams, and our conclusion supports the idea that kinetic effects are important and should not be neglected. We show that a deformation (leading either to a plateau or a beam) of the proton distribution function is a common consequence of the nonlinear trapping induced by parametric instabilities, where the acoustic modes generated by the instability of the mother Alfvén wave can enter in resonance with protons. We report an investigation for different plasma parameters, comparing left and right polarizations of the mother waves, from low plasma beta regimes to $\beta \geq 1$, and for both coherent (monochromatic) and incoherent initial Alfvén waves. A detailed analysis of the changes with respect to the fluid predictions introduced by kinetic effects on the instabilities for all the studied regimes is, however, beyond the aim of this work, and we address the reader to the papers just cited. In this study, we mainly focus on the properties of the wave-particle interactions induced by the instability dynamics and on the consequent departure from the Maxwellian equilibrium of the ion distribution function. In particular, we are interested in establishing when a velocity beam in the proton distribution is an expected result in terms of the main plasma parameters and wave properties.

[9] The paper is organized as follows: Section 2 reports results from hybrid simulations. First, in section 2.1, we discuss the dynamics of parametric instabilities in the case of a single monochromatic mother wave; then in section 2.2 we extend our study to the case of an incoherent spectrum of fluctuations. In section 3 we report the conclusion of our analysis and we discuss the possible application to space plasmas.

2. Simulation Results

[10] To investigate the dynamics of parametric instabilities when ion kinetic effects are retained, we performed 1-D numerical simulations using a hybrid code [*Matthews*, 1994] that treats protons as particles and electrons as a charge-neutralizing fluid with a constant temperature. In this framework it is possible to study wave-wave interactions as parametric instabilities, also taking into account the departure from the Maxwell-Boltzmann equilibrium of the ion distribution functions due to the nonlinear coupling between particles and waves. In the code, units of space and time are the ion inertial length c/ω_p and the inverse proton cyclotron frequency Ω_p^{-1}, respectively, where $\Omega_p = q_p B_o / m_p c$ and $\omega_p = (4\pi n q_p^2/m_p)^{1/2}$ is the proton plasma frequency; $\beta_{p,e} = 8\pi n k_B T_{p,e}/B_0^2$ is the plasma beta for a given plasma species, protons or electrons (k_B is the Boltzmann constant). Velocities are expressed in unit of the Alfvén velocity $v_a = B_0/(4\pi n m_p)^{1/2}$.

2.1. Monochromatic Wave

[11] We start our analysis by considering a coherent case: We study the parametric instability of a single monochromatic Alfvén wave propagating along the ambient magnetic field, which is taken along the x direction, and the nonlinear saturation of the associated growing compressive mode. Characteristics of simulations discussed in this paragraph are reported in Table 1. We report results for the cases most representative of the physics and dynamics of beam generation in the proton distribution evolution. Other numerical experiments that were performed in intermediate regimes of these plasma parameters, but not reported, confirm the results discussed here.

[12] We first consider the case of run A, where the initial Alfvén pump wave with $k_0 = 0.2$ is left-handed polarized and has an amplitude of $\delta B/B_0 = 0.05$. The total simulation box length, which is in the x direction, is 600 with $\Delta x = 1$, and there are 2×10^4 particles per cell (ppc); note that these values allow for a very good description of the particle distribution function with low numerical noise. The same resolution is adopted in all the simulations presented here. The proton beta is taken as $\beta_p = 0.01$ to study the parametric instability dynamic in a condition of low plasma beta, as is observed, for example, in the solar wind plasma at small heliocentric distances. Figure 1 (top) shows the time evolution of the RMS of density fluctuations. At $t = 0$, the density RMS shows simply a numerical noise owing to the discretization of the spatial grid, which is a feature typical of particle-in-cell (PIC) codes and which we keep low ($\sim 10^{-3}$) thanks to our choice of ppc. After time ~500, the level of density fluctuations starts to increase, owing to the growth of an acoustic-like compressive mode which interacts with the pump wave. At the same time, a reflected daughter

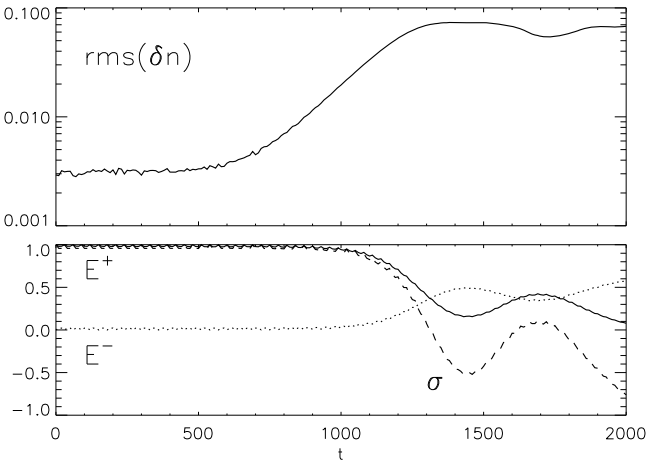

Figure 1. Parametric decay of a monochromatic Alfvén wave with left-handed polarization (run A). Temporal evolution of (top) RMS of density fluctuations and (bottom) wave energy of forward E^+ (solid line) and backward E^- (dotted line) propagating Alfvén waves [normalized to the initial mother wave energy $E_0 = E^+$ ($t = 0$)] and associated cross helicity σ(dashed line).

Alfvén wave develops, propagating in the opposite direction of the mother wave. To study the dynamics of the system it is useful to introduce the energy $E^+(E^-)$ associated with the forward (backward) Alfvén propagation, and the cross helicity $\sigma = (E^+ - E^-)/(E^+ + E^-)$, which is a measure of the prevailing mode: σ is zero when backward and forward propagating perturbations have the same energy, whereas it is equal to 1 when, as in the initial state of our simulation, the Alfvén wave is forward propagating. Figure 1 (bottom) shows the evolution of Alfvénic energies: E^+ (solid line) decreases as the mother wave is being damped, and E^- (dotted line), which is initially zero, increases, revealing the growth of a backward propagating daughter wave. Finally, the cross helicity (dashed line), initially equal to 1 because only E^+ is initialized in the simulation, switches to a negative value as E^- becomes larger than E^+. The result of this parametric decay can be described considering the wave spectrum as in Figure 2, where we report the magnetic field (solid), density (dashed), and parallel electric field (dotted) spectra of fluctuations at time 900, which according to Figure 1 corresponds to the phase of linear growth of the instability. The mother wave has wave number $m_0 = 20$, corresponding to the magnetic energy peak at $k \sim 0.2$, and initially no other signatures are present in the spectra. In Figure 2 we observe that the decay then generates a higher-frequency ($m_s = 31$) compressive acoustic-like wave, which produces a signal in the density and parallel electric field spectra for $k \sim 0.3$. According to the resonant condition for wave numbers, $m_s = m_0 + m_r$, we also observe a lower-frequency backward Alfvén wave with $m_r = 11$, which corresponds to the second peak in the transverse magnetic fluctuations at $k \sim 0.11$.

[13] At $t \sim 1300$, after the linear phase of growth of the acoustic mode, the instability saturates and the density stops increasing. However, some nonlinear interactions between the waves continue after the saturation, as suggested by the exchange of energy during the oscillatory postsaturation evolution of E^+ and E^-. In this kinetic regime the instability saturation is provided by particle trapping, because this is the main saturation process of unstable wave growing in collisionless plasmas. The interesting consequence of such a mechanism is that not only do kinetic effects change the wave-wave interactions and the saturation of the parametric decay with respect to fluid-case predictions [*Inhester*, 1990; *Vasquez*, 1995; *Araneda*, 1998; *Nariyuki and Hada*, 2006a, 2007; *Araneda et al.*, 2007], but, in particular, the ion dynamics can also be importantly affected by the trapping and by the wave-particle interactions deriving from the saturation phase of parametric instabilities. This is well illustrated by analyzing the evolution of the velocity distribution function. To study the role of ions in the saturation of the instability, we report in Figure 3 the proton distribution in the phase space x–v_x at different simulation epochs. The gray scale encodes the number of particles increasing from the darker gray and the solid line shows the corresponding density profile (in arbitrary units). Figures 3a and 3b refer to the linear phase of the instability. During this phase, density fluctuations driven by the unstable acoustic wave grow in amplitude. At wavefronts the parallel electric field produced by the compressive mode accelerates protons which are in resonance with the phase velocity of the wave. Figure 3c reports the proton distribution at $t = 1400$, when according to Figure 1 the saturation of the instability has taken place and density fluctuations have stopped their growth. The proton distribution shows phase space vortex structures, which are a typical signature of particle trapping; this confirms that the instability saturation occurs via trapping. The particle resonant with the wave has been accelerated, and this produces a population of faster protons. Figure 3d reports the proton characteristics during the postsaturation phase of the parametric decay. At this stage, the excited monochromatic acoustic wave starts to lose its coherence and the trapping wavefronts are destroyed. Trapped particles

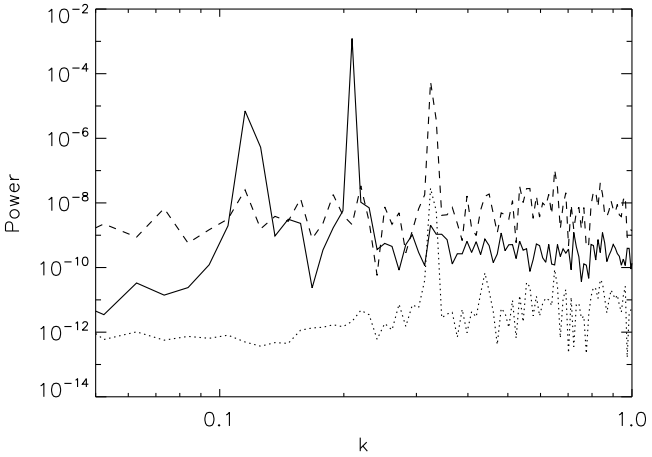

Figure 2. Magnetic field (solid line), density (dashed line), and parallel electric field (dotted line) spectra of fluctuations at time $t = 900$ for run A, corresponding to the linear phase of the parametric decay. Peaks in the magnetic field identify the mother and daughter backward propagating Alfvén waves at $k = 0.2$ and $k = 0.1$, respectively; the peak in the density and electric spectra at $k \sim 0.3$ corresponds to the growing ion acoustic mode.

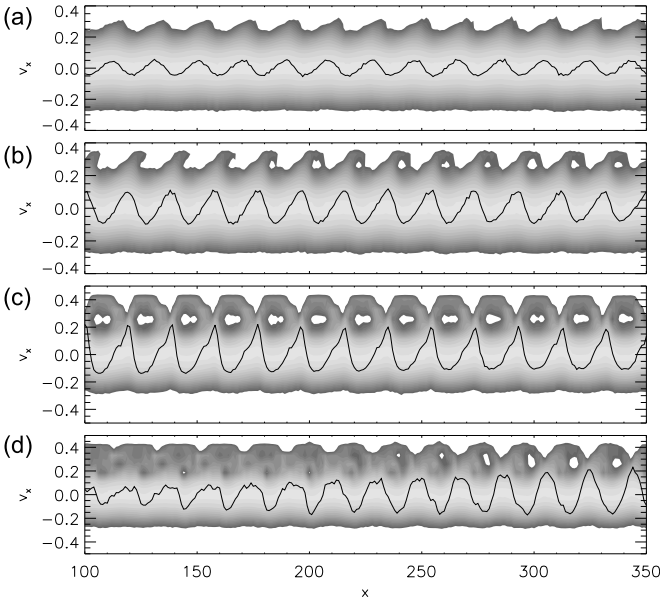

Figure 3. Proton phase space x–v_x in the case of the decay of a monochromatic Alfvén wave (run A). Different simulation times are as follows: (a) t = 900, (b) t = 1100, (c) t = 1400, and (d) t = 1800. The gray scale encodes the number of particles, increasing from the darker gray. The solid line shows (in arbitrary units) the corresponding density profile of the unstable compressive acoustic wave generated by the decay of the pump wave.

that are no longer confined by the electric potential then start to fill in the phase space and produce a ballistic velocity beam aligned with the ambient magnetic field, as shown in Figure 4.

[14] The heating of ions in the parallel direction as a consequence of the proton trapping in the parametric decay of a monochromatic Alfvén wave was noted in previous works of *Terasawa et al.* [1986] and *Vasquez* [1995]. However, these authors described it only in terms of a parallel temperature increase, owing to an enlargement of

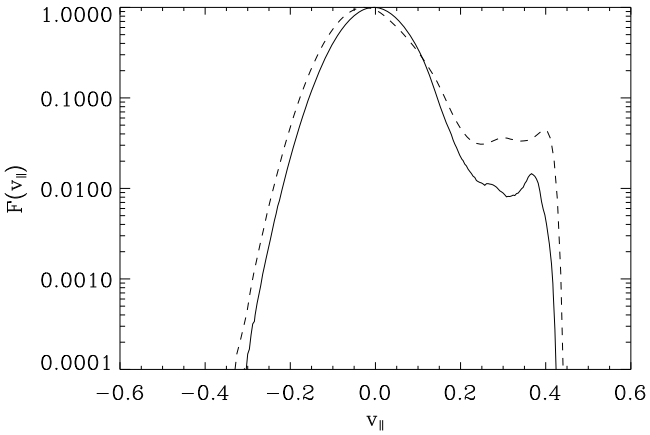

Figure 4. Final parallel distribution $f(v_\parallel)$ after the saturation of the parametric decay for run A (solid line) and run C (dashed line). The amplitudes of the mother wave are 0.05 and 0.1, respectively.

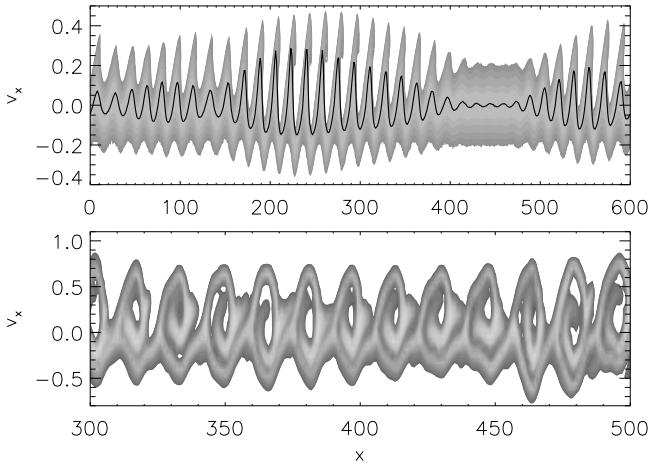

Figure 5. Proton phase space x–v_x in the case of the parametric decay of a large-amplitude mother wave, run E, with $\delta B/B_0$ = 0.5: (top) linear growth, t = 150, of the instability, where the solid line encodes the corresponding density profiles, and (bottom) detail of the phase space at saturation, t = 220.

the distribution function, whereas Figure 4 shows that this is a real proton acceleration, producing a forward propagating velocity beam. We repeated our study also for the parametric decay of an Alfvén wave with right polarization (run B) and obtained similar results as in the left-handed case; an analogous velocity beam is generated by the instability. This confirms that the trapping process and the proton acceleration are driven by the dynamics of the parametric decay, which for the conditions of those runs plays a role for both wave polarizations.

[15] Because the instability growth rate depends on the mother wave characteristics, increasing its amplitude, as in run C, produces a faster decay with a higher level of density fluctuations at the saturation. However, this has little influence on the phase velocity of the resulting acoustic wave, which is the parameter driving the resonance with protons, so increasing the mother wave amplitude does not importantly change the drift velocity of the resulting beam. Indeed, concerning the evolution of the proton distribution, the main difference of run C with respect to run A (see Figure 4) is only a more efficient trapping owing to the larger density fluctuations induced by the unstable ion-acoustic mode, leading to a more populated beam.

[16] Further increasing the amplitude of the mother wave, as in runs D and E, confirms that evolution. At the same time, we observe that when the mother wave has a larger amplitude, the decay excites a larger range of acoustic modes, leading to a broader spectrum of unstable density fluctuations in k-space. As a consequence, the derived density profile results are spatially modulated and this corresponds to a modulation in the enhancement of the parallel electric field, which accelerates the resonant protons. Figure 5 reports the parallel distribution in the phase space x–v_x for two simulation times in the case of run E, with a mother wave amplitude of $\delta B/B_0$ = 0.5. Figure 5 (top) shows the initial linear phase of the parametric decay instability, corresponding to the generation of density fluctuations that are modulated along x; we observe that the interaction and consequent

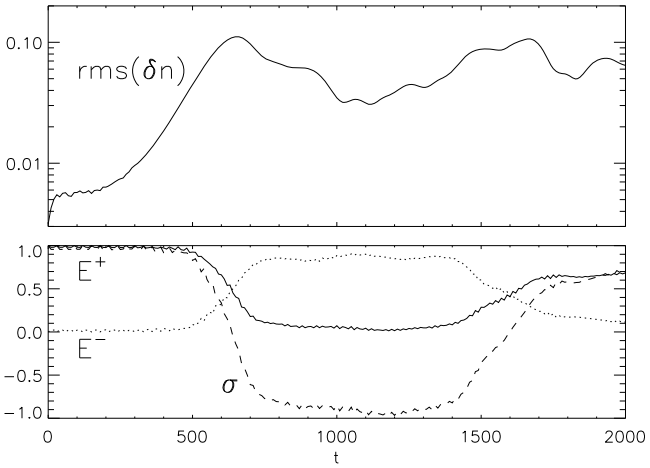

Figure 6. Parametric decay of a left-handed pump wave in the case of $T_e = 0$ (run F). (top) Density RMS evolution (as in Figure 1); (bottom) solid line, energy of the forward propagating waves (E^+); dotted line, energy of the backward propagating waves (E^-); dashed line, cross helicity σ.

deformation of the proton distribution are correlated to the enhancement of the density fluctuations and this produces different regions of particle acceleration. During the saturation of the instability, we observed the formation of regions of proton trapping, as reported in the detail of the phase space in Figure 5 (bottom), identified by the presence of phase-space vortices.

[17] To confirm the role of the parallel electric field generated by density fluctuations in the particle acceleration, we performed some simulations with $T_e \sim 0$ for the electronic fluid. As in the hybrid code in the electric field equation [*Matthews*, 1994, equation (15)]

$$\mathbf{E} = \frac{c}{4\pi}\frac{(\nabla \times \mathbf{B}) \times \mathbf{B}}{\rho_c} - \frac{\mathbf{J}_i \times \mathbf{B}}{\rho_c} - \frac{\nabla P_e}{\rho_c}, \qquad (1)$$

the term ∇P_e contributes to the total electric field via the particle density ($P_e = nk_B T_e$), taking cold electrons has the effect of decoupling the electric and density fluctuations. Despite the unphysical picture of these kinds of simulations, they are useful to identify the mechanism driving the instability saturation and beam formation. The results of one of these simulations, run F, with $\beta_e = 0$ and $\beta_p = 0.01$ are reported in Figure 6. The growth rate of the density mode and the decay rate of the mother Alfvén wave result changed with respect the case with warm electrons (Figure 1); this is because the instability growth rate depends on both the electron-proton temperature ratio and the total plasma β, which is the combination of β_e and β_p. However, the main consequence of $T_e = 0$ is the different saturation of the mother wave decay; the suppression of the electric field enhanced by the density fluctuations inhibits particle trapping as the saturation mechanism. Consequently, the decay of the initial Alfvén wave cannot be stopped and, for the choice of parameters displayed in Figure 6, it provides the total transfer of energy from the mother wave to the daughter wave at the same time that the cross helicity goes from 1 to −1. This dynamics allows for a later second parametric decay, where the previous backward daughter wave is now the pump wave and another forward wave grows in the system after $t = 1300$. At the end of the simulation we have again $\sigma \sim 1$ and almost all the magnetic energy is in the E^+ component. This behavior is analogous to that described by *Del Zanna et al.* [2001], who investigated the parametric decay of a large-amplitude Alfvén wave within the MHD framework. This suggests that some properties of the fluid wave-wave interactions can be recovered in our hybrid context using cold electrons, such as a case where the proton trapping, which is mainly responsible for the nonlinear kinetic evolution of the instability with respect to the MHD description, is not at work. As a consequence of the absence of the electric potential which provides the particle trapping, during the linear phase of the instability we do not observe any proton beam formation in the case $T_e = 0$. This peculiar difference between the two cases (beam formation if $T_e \neq 0$ and beam absence if $T_e = 0$) confirms that the proton acceleration along the magnetic field is because of particle trapping in the potential barriers of the parallel electric field carried by the growing longitudinal acoustic modes generated by parametric decay.

[18] Particle trapping is characteristic not only of the decay instability but also of other parametric instabilities, as the modulational instability. Because in this case the initial pump Alfvén wave interacts with density fluctuations and provides the growth of acoustic modes, we also expect to observe a similar dynamics (proton beam formation) when this instability is at work [*Araneda et al.*, 2008]. Alfvén waves are modulational unstable depending on their polarization and plasma beta. Fluid theory predicts the left-handed polarized wave to be decay and modulational unstable only for $\beta < 1$, while the right-handed Alfvén wave is modulational unstable when $\beta > 1$. Kinetic effects can change this picture; indeed, linear computations and hybrid simulations [*Nariyuki and Hada*, 2007] show a richer dynamics: left-handed modes can also show a modulational instability for $\beta > 1$ and, in the same beta regime, right-handed modes can be characterized by both decay and modulational instability. It is then possible, for some choice of parameters, to study the effects of the modulational instability when this is dominant with respect to the decay. We report as an example the results of a simulation (run G) of a right-handed pump wave, with $\delta B/B_0 = 0.5$ for $\beta_e = 4$ and $\beta_p = 0.1$. As in Figure 1, we report in Figure 7 the evolution of density fluctuations and of energies E^+ and E^-. The growth of density fluctuations (Figure 7, top) indicates that a parametric instability takes place, and this corresponds to a decreasing of the initial wave energy E^+ (solid line, Figure 7, bottom). Unlike the decay case, this process is not characterized by the generation of backward propagating waves; both E^- and the cross helicity σ (dashed line) remain almost constant. Figure 8 shows the magnetic (solid line), density (dashed line), and parallel electric field (dotted line) fluctuations spectrum, at time 1200, which according to Figure 7 corresponds to the linear growth of the instability. The initial mother wave has $k_0 = 0.2$ and is identified by the narrow peak in the magnetic spectrum. An acoustic mode with $k_s < k_0$, indicated by the peak in the density and electric field spectra, has developed, together with two Alfvén waves which propagate in the same direction as the mother wave and have their maximum at $k = k_s \pm k_0$ in the magnetic spectrum, corresponding to lower and upper sideband

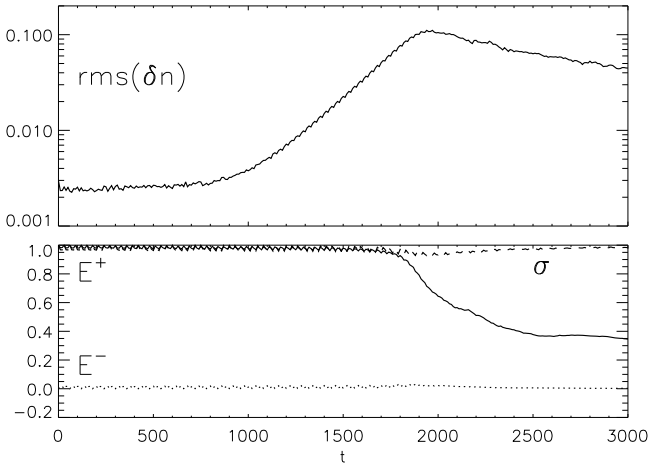

Figure 7. Results for run G, showing a modulational instability for an initial right-handed wave with $\beta_p = 0.1$ and $\beta_e = 4$: (top) density RMS (as in Figure 1); (bottom) evolution of E^+(solid line), E^-(dotted line), and σ(dashed line).

waves. All these properties identify the presence of a modulational instability.

[19] Also in this case density fluctuations grow and accelerate particles in a similar way as in the decay instability; the resulting evolution of the proton distribution function shows the presence of a velocity beam. Figure 9 reports the proton phase space x–v_x at different simulation times. As in Figure 3, these correspond to the linear, saturation, and postsaturation phases of the instability. Note that in this case, because the proton beta is larger than in previous simulations, the distribution function has a larger thermal width ($\beta_p \propto T_p$) and the interaction with the acoustic wave can then involve protons with larger velocities. As a consequence the particle resonance and acceleration are of the order of the Alfvén speed and it results in a beam traveling faster than v_a. This is interesting for space plasma in the solar wind, where proton velocity beams of the order of $\sim 1.5\ v_a$ are often observed [e.g., *Marsch et al.*, 1982].

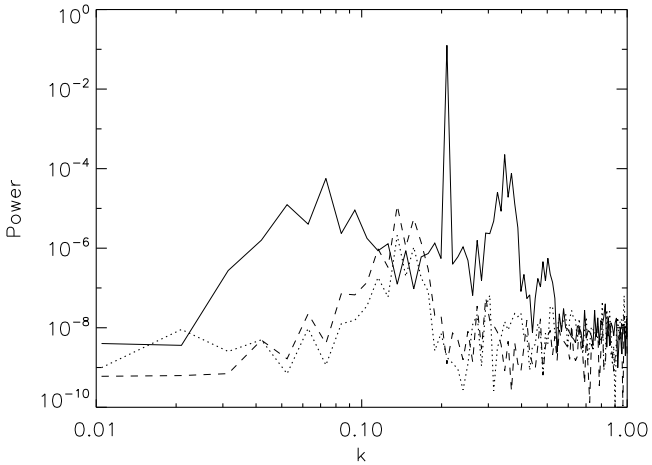

Figure 8. Spectrum of fluctuations at time 1200 for run G, corresponding to the modulational instability of a right-handed mother wave: solid line, magnetic fluctuations; dashed line, density; dotted line, parallel electric field.

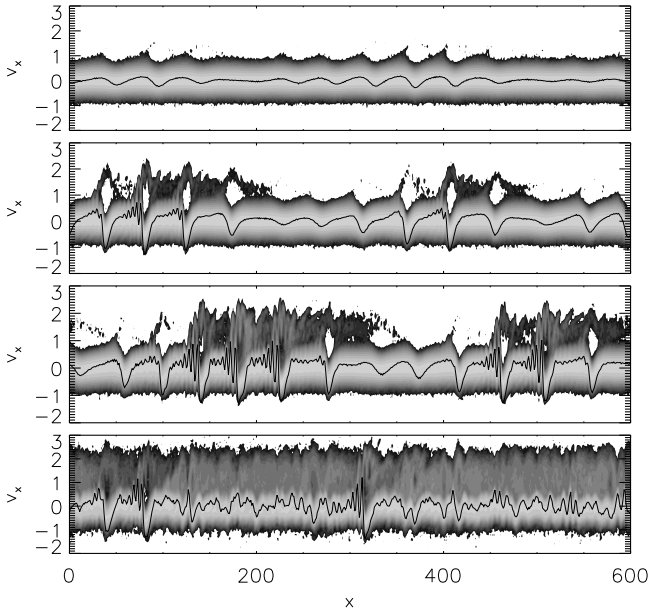

Figure 9. Proton phase space x–v_x for run G at different times: from top to bottom, t = 1500, 1800, 1900, and 2200. As in Figure 3, the gray scale encodes the number of particles increasing with darker gray and the solid line shows the corresponding density profile (in arbitrary units) of the unstable acoustic wave generated by the modulational instability.

[20] To conclude this section we focus on the final beam velocity properties obtained in our simulations, in particular on the possibility of developing beams that travel at the local Alfvén speed. We found that the proton beta β_p, together with β_e, plays a major role in the selection of the final beam velocity. This is because on one side the plasma beta directly influences the instability dynamics and has a role in selecting the phase velocity of the unstable acoustic mode; on the other side, β_p controls the thermal width of the distribution and shifts the position of the range of protons in resonance with the resulting acoustic mode. Resonant particles are mainly in the tails for a low-proton beta, whereas they are close to the thermal core for $\beta_p \sim 1$ or larger. We performed different runs with different values of β_p. Figure 10 reports the final proton distribution functions for runs H, I, and J, when the mother wave leads to a decay instability, a modulational instability, and a decay instability, respectively. Figure 10 reports the 2-D velocity distribution in the $v_\parallel$–$v_\perp$ plane ($v_\perp = \sqrt{v_y^2 + v_z^2}$) (left) and also shows the reduced parallel distribution $f(v_\parallel)$ (right). We observe that in the first two cases the instabilities develop a velocity beam; however, the third case results in a velocity plateau. Run H, which has $\beta_p = 0.8$, shows a dynamics very similar to that in run A with the decay instability which characterizes the evolution of the system. However, as in this case the proton beta is larger and the interaction between resonant protons and the ion-acoustic wave involves larger velocities than run A, the final beam has a larger drift velocity, which almost reaches the Alfvén speed. Further increasing β_p, as in run I, produces a still faster beam, which, thanks to the larger initial distribution temperature, can exceed v_a. We also have

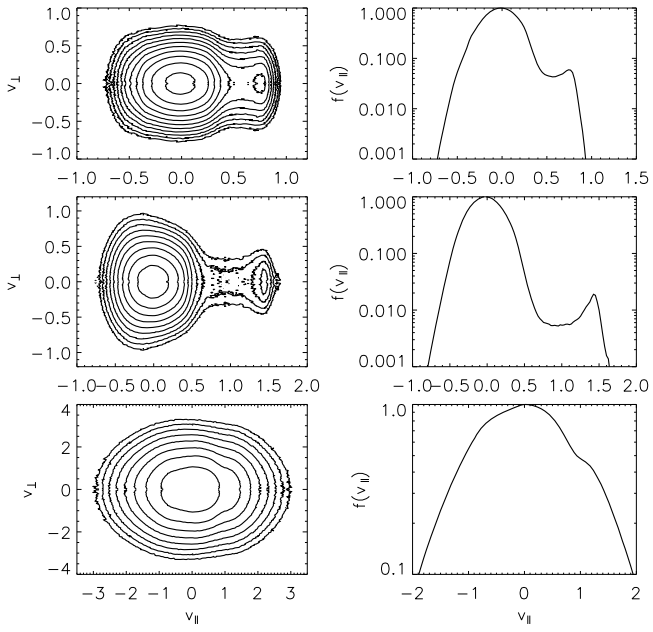

Figure 10. Final proton distribution function for different values of β_p after the saturation of a parametric instability (runs H, I, and J): (left) 2-D velocity distribution in the $v_\parallel$–$v_\perp$ plane and (right) reduced parallel distribution $f(v_\parallel)$.

to note that, in this case, the acceleration is provided by a modulational instability, which often destabilizes an acoustic wave having a larger phase velocity than in the decay case [*Araneda et al.*, 2009]. Finally, when the proton beta is of the order of 1, as in run J, the mechanism of beam production is not more efficient, as for these high temperatures the resonance between acoustic waves and ions falls closer to the thermal core of the distribution, and the resulting deformation leads to a plateau instead of a faster beam.

[21] Further simulations in a $\beta_p > 1$ regime (runs K and L) confirm that, despite the generations of acoustic modes owing to parametric instabilities, the proton distribution does not show the formation of a proton beam as in the $\beta_p < 1$ regime.

2.2. Spectrum of Waves

[22] In this section, we consider a more complex case, introducing a spectrum of Alfvén waves instead of a single monochromatic mode. The presence of several modes with different phases destroys the coherence of the single monochromatic wave and produces an initial modulation of the fluctuating magnetic field $B_\perp^2$ along the box. This introduces two important effects with respect to the previous section. The first is a fast increase of density fluctuations due to ponderomotive effects, which drives the plasma through the "static approximation" condition [*Spangler and Sheerin*, 1982; *Spangler*, 1989] with $n \propto B^2$.

[23] The second aspect is that the nonconstant profile of the magnetic field can lead to the formation and evolution of wave packets and these can then become modulational unstable [e.g., *Machida et al.*, 1987; *Vasquez*, 1993; *Velli et al.*, 1999; *Buti et al.*, 2000]. The further evolution of the modulation of B^2 can then break the static approximation, leading to a more complicated evolution [*Machida et al.*, 1987; *Nariyuki and Hada*, 2006b]. The modulational instability driven by incoherent modes can be an alternative channel for the mother wave energy dissipation, and for some range of parameters this can be dominant with respect to the instabilities predicted for coherent waves [*Nariyuki et al.*, 2007].

[24] We report the results from a simulation of an incoherent spectrum of Alfvén waves, which includes the effects just described but at the same time still recovers the main properties of the evolution found in section 2.1 for monochromatic waves. We adopt the same plasma parameters as in run A of section 2.1. The initial left-handed spectrum of Alfvén waves is composed of modes from $m = 10$ to $m = 20$, corresponding to wave vectors $0.1 < k < 0.2$, with amplitude $\delta B/B = 0.05$ for each mode and with random phases.

[25] Figure 11 reports the temporal evolution of the density RMS and Alfvénic energies E^+ and E^- as in Figure 1. In the first part of the simulation ($t < 100$, Figure 11, top), the density fluctuations quickly grow and reach a level of $\sim 5 \times 10^{-2}$ due to the ponderomotive effects.

[26] Then at $t \sim 600$, after a plateau phase in the RMS evolution, density fluctuations start to grow again. This time the growth corresponds to the generation of compressive acoustic modes provided by parametric decay. In this case, more modes are parametrically unstable at the same time, and this generates a spectrum of compressive growing modes interacting with the pump waves. At the same time, the energy of the forward propagating spectrum begins to decrease (solid line in Figure 11, bottom) and a spectrum of backward propagating waves starts to develop, as indicated by the evolution of E^- (dotted line). A trend similar to the monochromatic case can then be found (compare with Figure 1 for run A). The parametric decay then saturates when the two spectra have almost the same energy as the cross helicity goes to zero (dashed line). With respect to Figure 1, in this case the decay of the spectrum produces a smaller level of backward waves.

[27] The parametric decay of the initial incoherent spectrum of Alfvén waves is not the only instability taking place. Figure 12 shows the time stackplot of $B_\perp^2$ from $t = 0$ to $t = 1000$ with time steps of 50, in a framework moving at v_a.

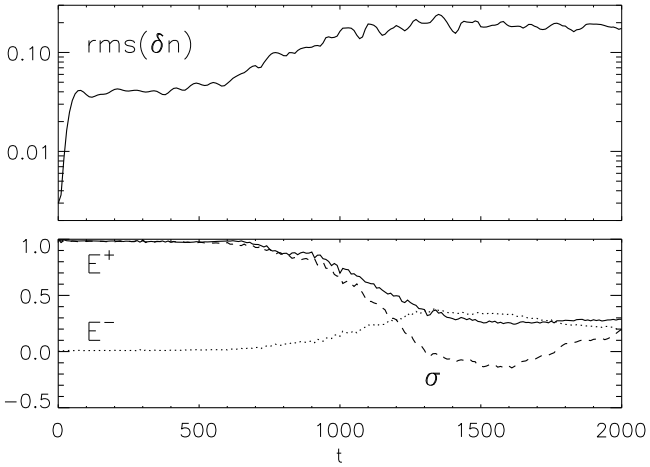

Figure 11. Time evolution of (top) the density RMS and (bottom) E^+ (solid line), E^- (dotted line), and σ (dashed line) for a spectrum of left-handed Alfvén waves.

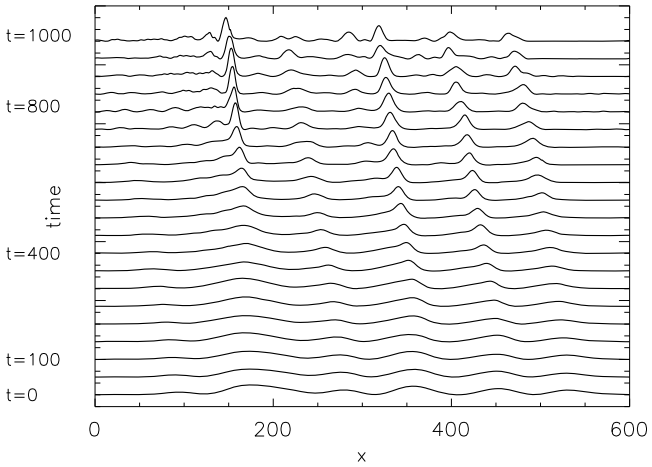

Figure 12. Time stackplot of the perpendicular magnetic field profile $B_\perp^2$ along the simulation domain x. The initial Alfvén wave train is left-handed and is modulational unstable. The temporal evolution is from $t = 0$ (bottom), to $t = 1000$ (top), with time steps of 50. Here a wave frame moving at v_a is adopted.

The shape of the magnetic field fluctuations is modulated by the phases of the initial spectrum, so some wave packets on $B_\perp$ are formed along x already at $t = 0$. These wave packets evolve in time: they shrink and grow in amplitude. This is in agreement with previous studies [e.g., *Buti et al.*, 2000; *Velli et al.*, 1999] and is the result of a modulational instability (which according to the theory is predicted to take place for our initial conditions: left-handed polarization and $\beta < 1$). At the same time, the local gradients of $B_\perp^2$ contribute to the enhancement of the parallel electric field. In equation (1), the total electric field E is the sum of three terms. The first term contributing to the electric field, $\hat{\mathbf{E}} \propto (\nabla \times \mathbf{B}) \times \mathbf{B}$, has for each component i the following form:

$$\hat{E}_i = -\frac{1}{2}\frac{\partial B_\perp^2}{\partial i} + B_j \frac{\partial B_i}{\partial_j} + B_k \frac{\partial B_i}{\partial k}, \tag{2}$$

with $B_\perp^2 = (B_j^2 + B_k^2)$. For an ambient magnetic field that depends only on one direction (e.g., x) with transverse fluctuations, equation (2) leads in the parallel direction to the simple expression

$$\hat{E}_\parallel(x) = -\frac{1}{2}\frac{\partial B_\perp^2}{\partial x}. \tag{3}$$

[28] Figure 13 reports the magnetic (solid line) and parallel electric field E_x (dashed line) profiles at time $t = 600$, when the decay instability has not yet taken place. We observe that the electric field is enhanced at the peaks of $B_\perp^2$ and that the correlation between magnetic and parallel electric field is well in agreement with equation (3). The generation of a parallel electric field in this phase can eventually also produce a proton acceleration; we discuss in more detail the effects of unstable wave packet evolution, growth, and collapse, as well their role in accelerating velocity beams, in another work (M. Velli et al., Dispersive effects and nonlinearities: Decay of Alfvénic solitons and instabilities of phase modulated wave packets, in preparation, 2010).

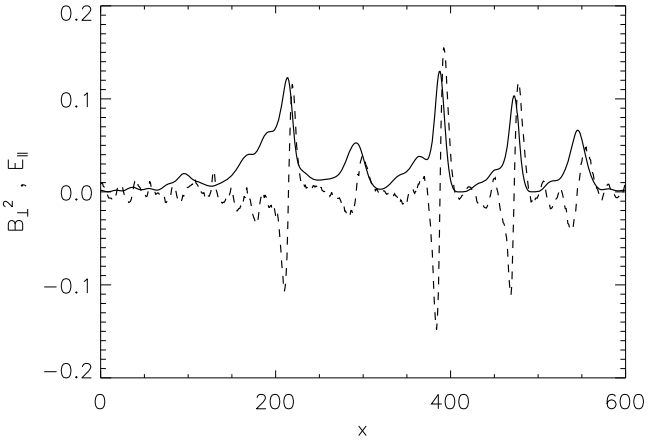

Figure 13. Magnetic fluctuations $B_\perp^2$ (solid line) and parallel electric field (dashed line) profiles at $t = 600$ for the left-handed spectrum of Figure 11.

[29] After $t \sim 600$, when the decay instability also takes place, both processes contribute to the electric field, which accelerates ions. Figure 14 shows the evolution of the proton phase space and the corresponding density (solid line) and magnetic field (dashed line) profiles at different simulation times. Figure 14a refers to time $t = 600$ when, according to Figure 13, the parallel component of the electric field is driven by the gradients of $B_\perp$. Figures 14b–14d report the proton distribution at times $t = 800$, 900, and 1000, respectively, corresponding to the linear phase and saturation of the decay instability, leading to the growth of ion-acoustic modes that generate density fluctuations. The global result is analogous to the result in section 2.1, with

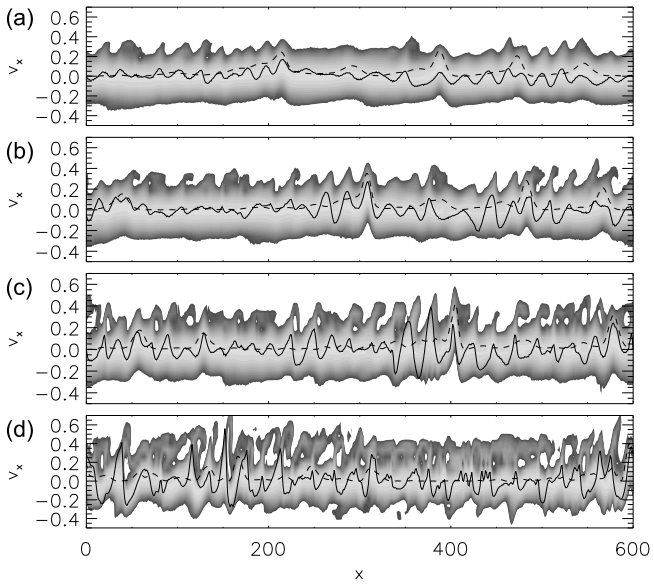

Figure 14. Proton phase space x–v_x, as in Figure 3, at times (a) $t = 600$, (b) $t = 800$, (c) $t = 900$, and (d) $t = 1000$ in the presence of a spectrum of Alfvén waves. The density and perpendicular magnetic field $B_\perp^2$ profiles are also reported as solid and dashed lines, respectively.

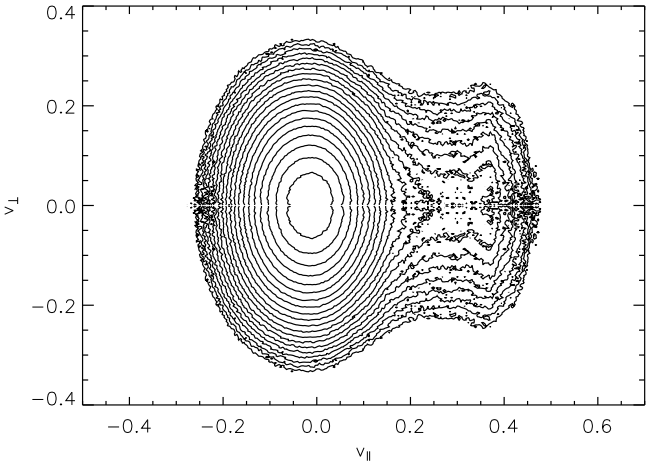

Figure 15. Proton distribution function $f(v_{\parallel},v_{\perp})$ resulting from the parametric instability of a spectrum of left-handed Alfvén waves.

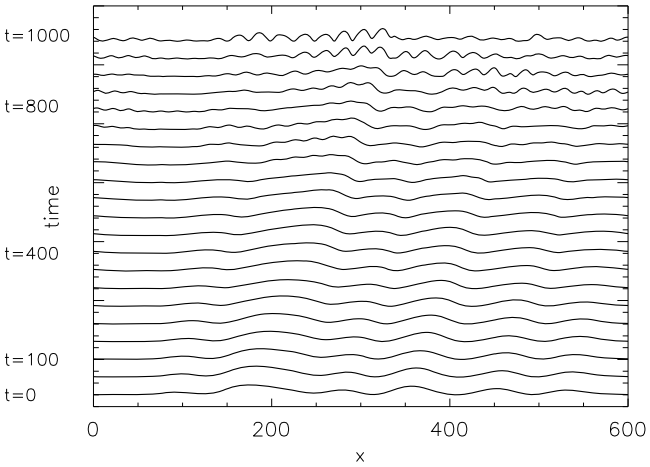

Figure 17. Time stackplot of $B_{\perp}^2$ as in Figure 12 but for right polarization. The initial Alfvén wave train is not modulational unstable.

the acceleration and formation of faster streams in the proton phase space. The resulting proton distribution function in velocity space, $f(v_{\parallel},v_{\perp})$, is reported in Figure 15 and it shows the generation of a velocity beam for $v_{\parallel} > 0$. The analysis of the temporal evolution of the proton distribution shown in Figure 14 allows one to compare the role of magnetic and density gradients in the particle acceleration. The shape of the proton distribution suggests that the main contribution derives from the acoustic fluctuations (solid line) generated by the instabilities after time ~800, in a way analogous to the monochromatic case.

[30] The importance of density gradients in accelerating a velocity beam is confirmed by the results obtained by repeating the same simulation for a right-handed spectrum and reported in Figure 16. The density RMS (Figure 16, top) follows a temporal evolution very similar to that observed in the left-handed case (Figure 11), with the fast increase of density fluctuations driven by ponderomotive effects, a plateau phase, and then the linear growth of a parametric instability, followed by its saturation at $t \sim 1000$. According to the evolution of the forward and backward propagating wave energies, the parametric process can be identified (Figure 16, bottom) as a decay instability, as in the left-handed case. Note that this is also in agreement with the monochromatic results of run B, where for the same plasma conditions the coherent right-handed mother wave resulted subject to the parametric decay.

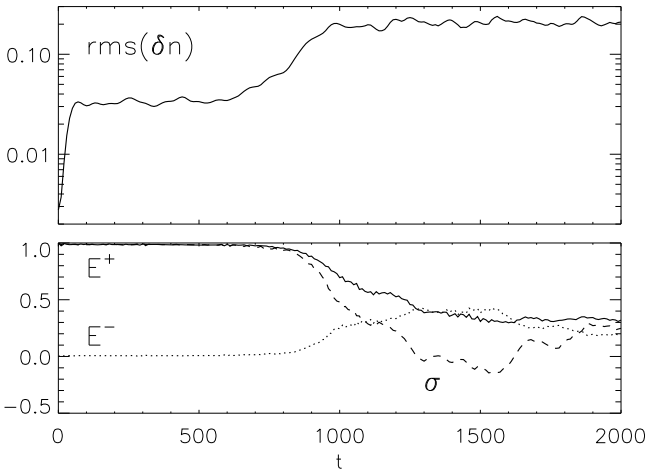

Figure 16. Time evolution of the parametric instability of a spectrum of right-handed Alfvén waves: (top) density RMS and (bottom) evolution of E^+, E^-, and σ as in Figure 11.

[31] There is, however, a relevant difference with the previous case of left polarization. Even if linear theories, which include finite proton temperature effects, predict a modulational instability also for right-handed Alfvén waves at $\beta < 1$ [*Nariyuki and Hada*, 2006a; *Araneda et al.*, 2007], with the values of β_p and β_e adopted here, the decay instability results as the dominant mechanism [*Nariyuki and Hada*, 2006a; *Nariyuki et al.*, 2007, 2008a]. Consequently, in the case of a right-handed spectrum, after the initial growth of density fluctuations due to the ponderomotive force, we do not recover the evolution of $B_{\perp}^2$ found in Figure 12 for the left polarization. Figure 17 shows that in the right-handed case wave packets do not shrink and grow in amplitude, but on the contrary are slowly dispersed at later times. On the other hand, because the plasma is found to be unstable for decay instability, we observe the generation of acoustic waves, the enhancement of the parallel electric field trapping the protons, and the consequent acceleration, as in the case of an incoherent left-handed spectrum. It results in a final proton distribution with a velocity beam analogous to that in Figure 15 also for the right-handed spectrum. This confirms that for the range of parameters investigated here the formation of a proton beam is driven by density gradients, in a similar way for both polarizations and in agreement with the results of the previous section.

[32] We extended our analysis to the case of a broader band initial spectrum. We repeated the previous simulations for both left and right polarization, introducing initial spectra of 30 modes from $k = 0.1$ to $k = 0.4$ and 50 modes from $k = 0.01$ to $k = 0.5$. The results obtained confirm that the mother wave energy is dissipated by parametric instabilities: the RMS of density fluctuations increases and some fraction of backscattered waves is generated by the coupling. However, in agreement with *Nariyuki et al.*

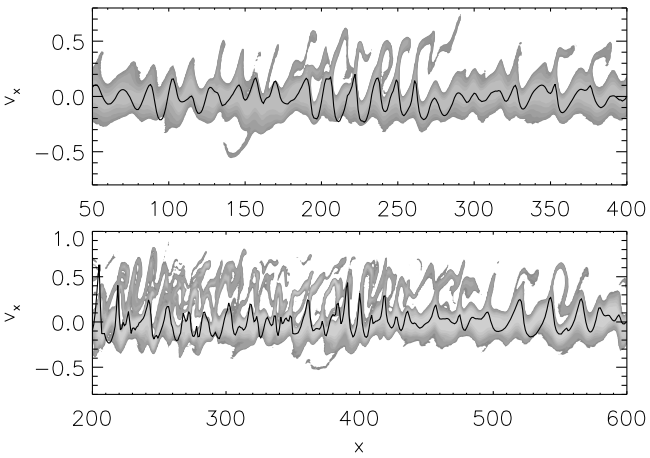

Figure 18. Zoom of the proton phase space x–v_x at time t = 200 (top) and t = 300 (bottom) for a simulation with a large broadband initial spectrum, $0.1 < k < 0.4$. Solid line indicates the density profile corresponding to the fluctuations excited by parametric couplings.

[2008a], we observe a gradual decreasing of the level of fluctuations generated by the decay instability with the increasing bandwidth of the spectra. Nevertheless, during the linear growth of the instability, we observe a deformation of the proton distribution, with some parallel acceleration as in simulations with the narrower spectrum. Figure 18 reports the proton distribution in the phase space in the case of a simulation with a left-handed spectrum with $0.1 < k < 0.4$. The resulting evolution is qualitatively similar to Figure 14, showing localized proton acceleration by wavefronts of density fluctuations at time t = 200 (Figure 14, top) and, consequently, at t = 300, some signatures of incoherent trapping (Figure 14, bottom), leading then to the saturation of the instability. As a result, the proton distribution is characterized by the generation of a velocity beam as in Figure 15 for the narrower spectrum.

3. Conclusion

[33] In this study, we discussed the role of parametric instabilities in the evolution of proton distribution functions in a kinetic regime using the framework of a hybrid numerical code. In particular, we investigated the properties of the wave-particle interactions induced by the instability dynamics and their consequences on the ion distribution function. We found that both decay and modulational instabilities play a role in shaping the ion distributions, introducing nonthermal effects and providing departures from the initial Maxwellian shape. The final distributions resulting after the instability saturation show the presence of a parallel heating of protons provided by the resonant interaction with the ion-acoustic waves generated by the parametric coupling. The heating of the proton distribution along the magnetic field corresponds to the formation of either a plateau or a velocity beam, depending on the plasma beta regime that characterizes the plasma. This can be roughly understood by considering that the resonant acceleration is driven by the interaction between the phase velocity of the unstable acoustic mode and protons in resonance with it; both these quantities are mainly influenced by β_p. We performed different simulations of various beta regimes, finding that the most favorable condition for the formation of a well-developed proton beam is when $\beta_p < 1$. In particular, a beam with a velocity of the order of the local Alfvén speed is obtained for $\beta_p \sim 0.1$, in agreement with the work of *Araneda et al.* [2008]. Slower beams are observed for lower values of β_p, whereas when the proton beta approaches unity, the consequent thermal spread of the distribution moves the resonance into the distribution core ($v_a \sim v_{th,p}$) and a plateau results.

[34] Following the evolution of the proton distribution in the phase space during the development of the instability, we studied in detail the mechanism driving the generation of faster beams, which is controlled by the trapping potential of the ion-acoustic modes excited by the instability. Simulations including cold electrons where the electric field induced by the density fluctuations of the unstable compressive modes is suppressed and then the particle trapping is avoided do not recover the acceleration of resonant protons. On the contrary, as the amplitude of the mother wave is increased, leading to a larger level of density fluctuations, the trapping is improved and a more populated beam is generated by the interaction with the ion-acoustic mode.

[35] We extended our study to nonmonochromatic conditions, introducing a spectrum of Alfvén waves. The presence of an incoherent spectrum of fluctuations introduces some changes in the instability evolution with respect the coherent case [*Nariyuki et al.*, 2007]. The initial modulation of the magnetic field profile along the simulation box very quickly produces some macroscopic density fluctuations due to ponderomotive effects. The plasma then reaches the equilibrium given by the static approximation [*Spangler and Sheerin*, 1982] and density perturbations do not grow further until a parametric instability of the mother waves generating acoustic modes takes place at a later time. The evolution of the parametric coupling and instability is then similar to the analogous monochromatic case (with same plasma conditions and amplitude of the mother wave), with a linear phase of growth for daughter waves and the generation of backward propagating Alfvén waves in the case of a decay instability. At the same time, another effect characterizes the evolution of incoherent wave packets in the case when the plasma is unstable for modulational instability; wave packets are observed to evolve, grow in amplitude, and shrink [*Velli et al.*, 1999; *Buti et al.*, 2000], with a consequent enhancement of the electric field associated with the gradient of $B_\perp^2$. In our simulations, this electric field is not dominant with respect to the one driven by the generation of ion-acoustic modes. On the other hand, this can play a role in the evolution of Alfvénic solitons and large-amplitude wave packets; we address this problem in more detail in another study in preparation.

[36] Concerning the evolution of an incoherent wave spectrum, we find that, for the parameters adopted in our analysis, despite the presence of a modulational instability for the wave envelope which contributes to the dissipation of the initial mother wave energy, the decay instability of the initial spectrum influences the ion acceleration. We finally observe, for both polarizations, the growth of density fluctuations generated by the instability which then enter in resonance with protons and produce a velocity beam in the

particle distribution function. This evolution is confirmed also when larger broadband initial spectra are used.

[37] Our conclusion is that wave-wave couplings leading to the generation of compressive fluctuations and density gradients providing a nonlinear trapping of resonant particles can, in general, play a role in accelerating ion beams in plasmas. If this is the case, one could then also suggest that, independently from their excitation by parametric instabilities, the presence of ion-acoustic waves with a phase velocity in resonance with protons is, especially for low-beta plasmas (i.e., $\beta_p < 1$), a possible explication for the presence of proton secondary beams. Our study also offers a possible interpretation concerning some of the results of *Valentini et al.* [2008], who by studying the excitation of ion-acoustic wave activity through some three-wave couplings due to the nonlinear evolution of an Alfvénic turbulent cascade observed the generation of a velocity beam in the proton distribution function. Also, the plasma conditions adopted in their work, $\beta_p < 1$ and $T_e > T_p$, are in agreement with the conditions for a beam generation discussed in this work.

[38] The scenario obtained in this work is compatible with solar wind observations, where velocity beams are often observed in proton distribution functions [*Marsch et al.*, 1982]. These structures are aligned along the ambient magnetic field and have a typical velocity drift with respect the rest of the distribution of the order of the local Alfvén speed. The drift velocity is observed to be correlated with the proton beta [*Tu et al.*, 2004], in agreement with our conclusions. Following this interpretation it is likely that observing secondary proton beams with a drift speed of the order of the Alfvén speed is just a consequence of the fact that the plasma proton beta in the fast solar wind is <1 between 0.3 and 1 AU [e.g., *Matteini et al.*, 2007]. On the other side, parametric instabilities are believed to play a role in the solar wind, because an important flux of outward Alfvén waves ($E^+ > E^-$) is observed and it evolves with increasing heliocentric distance [*Bavassano et al.*, 2000]. However, the observed evolution of E^-/E^+, as well its possible association with the presence of ion velocity beams, has not yet been fully explained and remains an open question; further observational work is needed to determine the role of the parametric instabilities in the solar wind.

[39] At the same time, ion-acoustic waves are also observed in the solar wind [*Gurnett et al.*, 1979]. The role of these waves remains unclear because they are predicted to propagate only if $T_e \gg T_p$ and to beheavily damped for $T_e \sim T_p$; in the solar wind the electron-proton temperature ratio is observed to vary mainly in the range $0.5 < T_p/T_e < 4$ [*Schwenn and Marsch*, 1991], with $T_e < T_p$ in fast streams, and so in apparent contrast with the theoretical expectation. In this study we have taken, in agreement with other simulation investigations [*Araneda et al.*, 2008; *Valentini et al.*, 2008], $T_e > T_p$ to avoid the linear damping predicted by the theory. On the other hand, the ion-acoustic modes are nonlinearly driven so that the linear condition for their existence, $T_e \gg T_p$, is not necessarily relevant. Further investigations with $T_e/T_p \sim 1$, including the direct competition between linear damping and nonlinear generation by parametric instabilities, should be performed to link the present work to the solar wind framework in more detail; this point is the objective of future studies.

[40] Our work results are consistent with the study of *Markovskii et al.* [2009] on the effects of wave-wave couplings and wave dissipation of parallel propagating Alfvén waves in the context of coronal holes heating and solar wind acceleration. The presence of a parallel heating observed by the authors, and which appears to be associated to a parametric decay activity, could be the signature of the formation of a velocity beam in the proton distribution as our simulations at low proton andelectron plasma betas suggest.

[41] This work reports 1-D simulations; preliminary results performed using 2-D hybrid simulations but maintaining parallel propagation for the initial Alfvén waves confirm the present results. This is in agreement with the 2-DPIC simulation results of *Nariyuki et al.* [2008b], who found that compressive parallel ion-acoustic modes are preferentially generated by parametric instabilities also in two dimensions. However, oblique modes can play some role and more detailed 2-D studies including nonparallel propagation are planned.

[42] **Acknowledgments.** The research described in this paper was carried out in part at the Jet Propulsion Laboratory, California Institute of Technology, under a contract with the National Aeronautics and Space Administration. It was also supported by the Italian Space Agency contract ASI I/015/07/0 "Solar System Exploration." We thank Luca Del Zanna and André Mangeney for useful discussions during the preparation of the manuscript.

[43] Philippa Browning thanks Yasuhiro Nariyuki and another reviewer for their assistance in evaluating this manuscript.

References

Araneda, J. A. (1998), Parametric instabilities of parallel-propagating Alfvén waves: Kinetic effects in the MHD-model, *Phys. Scr. T*, *75*, 164–168, doi:10.1238/Physica.Topical.075a00164.

Araneda, J. A., E. Marsch, and A. F. Viñas (2007), Collisionless damping of parametrically unstable Alfvén waves, *J. Geophys. Res.*, *112*, A04104, doi:10.1029/2006JA011999.

Araneda, J. A., E. Marsch, and A. F. Viñas (2008), Proton core heating and beam formation via parametrically unstable Alfvén-cyclotron waves, *Phys. Rev. Lett.*, *100*(12), 125003, doi:10.1103/PhysRevLett.100.125003.

Araneda, J. A., Y. Maneva, and E. Marsch (2009), Preferential heating and acceleration of αparticles by Alfvén-cyclotron waves, *Phys. Rev. Lett.*, *102*(17), 175001, doi:10.1103/PhysRevLett.102.175001.

Bavassano, B., E. Pietropaolo, and R. Bruno (2000), On the evolution of outward and inward Alfvénic fluctuations in the polar wind, *J. Geophys. Res.*, *105*, 15,959–15,964, doi:10.1029/1999JA000276.

Belcher, J. W., and L. Davis Jr. (1971), Large-amplitude Alfvén waves in the interplanetary medium, 2, *J. Geophys. Res.*, *76*, 3534–3563.

Bruno, R., and V. Carbone (2005), The solar wind as a turbulence laboratory, *Living Rev. Sol. Phys.*, *2*, lrsp-2005-4.

Buti, B., M. Velli, P. C. Liewer, B. E. Goldstein, and T. Hada (2000), Hybrid simulations of collapse of Alfvénic wave packets, *Phys. Plasmas*, *7*, 3998–4003, doi:10.1063/1.1289890.

Del Zanna, L. (2001), Parametric decay of oblique arc-polarized Alfvén waves, *Geophys. Res. Lett.*, *28*, 2585–2588.

Del Zanna, L., M. Velli, and P. Londrillo (2001), Parametric decay of circularly polarized alfvén waves: Multidimensional simulations in periodic and open domains, *Astron. Astrophys.*, *367*, 705–718.

Derby, N. F., Jr. (1978), Modulational instability of finite-amplitude, circularly polarized Alfven waves, *Astrophys. J.*, *224*, 1013–1016, doi:10.1086/156451.

Ghosh, S., A. F. Vinas, and M. L. Goldstein (1993), Parametric instabilities of a large-amplitude circularly polarized Alfvén wave: Linear growth in two-dimensional geometries, *J. Geophys. Res.*, *98*, 15,561–15,570, doi:10.1029/93JA01534.

Goldstein, M. L. (1978), An instability of finite amplitude circularly polarized Alfvén waves, *Astrophys. J.*, *219*, 700–704, doi:10.1086/155829.

Gurnett, D. A., E. Marsch, W. Pilipp, R. Schwenn, and H. Rosenbauer (1979), Ion acoustic waves and related plasma observations in the solar wind, *J. Geophys. Res.*, *84*, 2029–2038.

Hasegawa, A. (1970), Stimulated modulational instabilities of plasma waves, *Phys. Rev. A*, *1*(6), 1746–1750, doi:10.1103/PhysRevA.1.1746.

Hasegawa, A. (1972), Theory and computer experiment on self-trapping instability of plasma cyclotron waves, *Phys. Fluids*, *15*, 870–881, doi:10.1063/1.1693996.

Hollweg, J. V. (1994), Beat, modulational, and decay instabilities of a circularly polarized Alfvén wave, *J. Geophys. Res.*, *99*, 23,431–23,447.

Hoshino, M., and M. L. Goldstein (1989), Time evolution from linear to nonlinear stages in magnetohydrodynamic parametric instabilities, *Phys. Fluids B*, *1*, 1405–1415, doi:10.1063/1.858971.

Inhester, B. (1990), A drift-kinetic treatment of the parametric decay of large-amplitude Alfvén waves, *J. Geophys. Res.*, *95*, 10,525–10,539.

Landi, S., and F. G. E. Pantellini (2003), Kinetic simulations of the solar wind from the subsonic to the supersonic regime, *Astron. Astrophys.*, *400*, 769–778.

Lashmore-Davies, C. N. (1976), Modulational instability of a finite amplitude Alfvén wave, *Phys. Fluids*, *19*, 587–589, doi:10.1063/1.861493.

Longtin, M., and B. U. O. Sonnerup (1986), Modulation instability of circularly polarized Alfvén waves, *J. Geophys. Res.*, *91*, 6816–6824, doi:10.1029/JA091iA06p06816.

Machida, S., S. R. Spangler, and C. K. Goertz (1987), Simulation of amplitude-modulated circularly polarized Alfvén waves for beta less than one, *J. Geophys. Res.*, *92*, 7413–7422, doi:10.1029/JA092iA07p07413.

Malara, F., and M. Velli (1996), Parametric instability of a large-amplitude nonmonochromatic Alfvén wave, *Phys. Plasmas*, *3*, 4427–4433.

Malara, F., L. Primavera, and P. Veltri (2000), Nonlinear evolution of parametric instability of a large-amplitude nonmonochromatic Alfvén wave, *Phys. Plasmas*, *7*, 2866–2877, doi:10.1063/1.874136.

Markovskii, S. A., B. J. Vasquez, and J. V. Hollweg (2009), Proton heating by nonlinear field-aligned Alfvén waves in solar coronal holes, *Astrophys. J.*, *695*, 1413–1420, doi:10.1088/0004-637X/695/2/1413.

Marsch, E., R. Schwenn, H. Rosenbauer, K.-H. Muehlhaeuser, W. Pilipp, and F. M. Neubauer (1982), Solar wind protons: Three-dimensional velocity distributions and derived plasma parameters measured between 0.3 and 1 AU, *J. Geophys. Res.*, *87*, 52–72.

Matteini, L., S. Landi, P. Hellinger, F. Pantellini, M. Maksimovic, M. Velli, B. E. Goldstein, and E. Marsch (2007), Evolution of the solar wind proton temperature anisotropy from 0.3 to 2.5 AU, *Geophys. Res. Lett.*, *34*, L20105, doi:10.1029/2007GL030920.

Matthews, A. P. (1994), Current advance method and cyclic leapfrog for 2D multispecies hybrid plasma simulations, *J. Comput. Phys.*, *112*, 102–116.

Mio, K., T. Ogino, S. Takeda, and K. Minami (1976), Modulational instability and envelope-solitons for nonlinear Alfvén waves propagating along the magnetic field in plasmas, *J. Phys. Soc. Jpn.*, *41*, 667–673.

Mjolhus, E. (1976), On the modulational instability of hydromagnetic waves parallel to the magnetic field, *J. Plasma Phys.*, *16*, 321–334.

Nariyuki, Y., and T. Hada (2006a), Kinetically modified parametric instabilities of circularly polarized Alfvén waves: Ion kinetic effects, *Phys. Plasmas*, *13*, 124501, doi:10.1063/1.2399468.

Nariyuki, Y., and T. Hada (2006b), Remarks on nonlinear relation among phases and frequencies in modulational instabilities of parallel propagating Alfvén waves, *Nonlinear Processes Geophys.*, *13*, 425–441.

Nariyuki, Y., and T. Hada (2007), Consequences of finite ion temperature effects on parametric instabilities of circularly polarized Alfvén waves, *J. Geophys. Res.*, *112*, A10107, doi:10.1029/2007JA012373.

Nariyuki, Y., T. Hada, and K. Tsubouchi (2007), Parametric instabilities of parallel propagating incoherent Alfvén waves in a finite ion beta plasma, *Phys. Plasmas*, *14*(12), 122110, doi:10.1063/1.2824986.

Nariyuki, Y., T. Hada, and K. Tsubouchi (2008a), On nonlinear evolution of Alfvénic turbulence in low beta plasmas, *Phys. Plasmas*, *15*(11), 114502, doi:10.1063/1.3028316.

Nariyuki, Y., S. Matsukiyo, and T. Hada (2008b), Parametric instabilities of large-amplitude parallel propagating Alfvén waves: 2D PIC simulation, *New J. Phys.*, *10*(8), 083,004, doi:10.1088/1367-2630/10/8/083004.

Sagdeev, R. Z., and A. A. Galeev (1969), *Nonlinear Plasma Theory*, Benjamin, New York.

Schwenn, R., and E. Marsch (1991), *Physics of the Inner Heliosphere II. Particles, Waves and Turbulence*, vol. 2, 1st ed., Springer.

Spangler, S. R. (1989), Kinetic effects of Alfvén wave nonlinearity: I. Ponderomotive density fluctuations, *Phys. Fluids B*, *1*, 1738–1746, doi:10.1063/1.858901.

Spangler, S. R., and J. P. Sheerin (1982), Properties of Alfvén solitons in a finite-beta plasma, *J. Plasma Phys.*, *27*, 193–198.

Terasawa, T., M. Hoshino, J.-I. Sakai, and T. Hada (1986), Decay instability of finite-amplitude circularly polarized Alfven waves: A numerical simulation of stimulated Brillouin scattering, *J. Geophys. Res.*, *91*, 4171–4187.

Tu, C.-Y., E. Marsch, and Z.-R. Qin (2004), Dependence of the proton beam drift velocity on the proton core plasma beta in the solar wind, *J. Geophys. Res.*, *109*, A05101, doi:10.1029/2004JA010391.

Umeki, H., and T. Terasawa (1992), Decay instability of incoherent Alfven waves in the solar wind, *J. Geophys. Res.*, *97*, 3113–3119, doi:10.1029/91JA02967.

Valentini, F., P. Veltri, F. Califano, and A. Mangeney (2008), Cross-scale effects in solar-wind turbulence, *Phys. Rev. Lett.*, *101*(2), 025006, doi:10.1103/PhysRevLett.101.025006.

Vasquez, B. J. (1993), Strongly nonlinear evolution of low-frequency wave packets in a dispersive plasma, *Phys. Fluids B*, *5*, 2021–2035, doi:10.1063/1.860789.

Vasquez, B. J. (1995), Simulation study of the role of ion kinetics in low-frequency wave train evolution, *J. Geophys. Res.*, *100*, 1779–1792.

Velli, M., B. Buti, B. E. Goldstein, and R. Grappin (1999), Propagation and disruption of Alfvénic solitons in the expanding solar wind, *AIP Conf. Proc.*, *471*, 445–448, doi:10.1063/1, 58837.

P. Hellinger, Astronomical Institute, Academy of Sciences of the Czech Republic, Bocni II/1401, 14131, Prague, Czech Republic.

S. Landi, Dipartimento di Astronomia e Scienza dello Spazio, Università degli Studi di Firenze, Largo E. Fermi 2, I-50125 Firenze, Italy.

L. Matteini, LESIA, Observatoire de Paris, 5 Place Jules Janssen, F-92195 Meudon, France. (matteini@arcetri.astro.it)

M. Velli, Jet Propulsion Laboratory, California Institute of Technology, 4800 Oak Grove Dr., Pasadena, CA 91109, USA.